Rheol Acta (2007) 46:629–637
DOI 10.1007/s00397-006-0147-6

ORIGINAL CONTRIBUTION

Shear banding during nonlinear creep with a solution of monodisperse polystyrene

Thomas Schweizer

Received: 30 May 2006 / Accepted: 18 September 2006 / Published online: 17 November 2006

Abstract Creep experiments with a solution of polystyrene (M_w=2.6 MDa, 16 vol.%, 25 °C) in diethyl phthalate are reported for stresses between 100 and 2,500 Pa ($\approx 3G_N^0/4$). The aim was to look for a flow transition as reported for strongly entangled poly(isobutylene) solutions. The experiments with the polystyrene solution were repeated for cone angles of 2, 4, and 6° (radius 15 mm) and showed no dependence on cone angle. The Cox–Merz rule was not fulfilled for stresses beyond about 800 Pa. The tangential observation with a CCD camera showed that the edge took a concave shape because of the second normal stress difference. Beyond 1,000 Pa, the concave edge develops into a crevice, thus substantially reducing the effective cross-section. This leads to runaway in a constant torque experiment. At p_{21}=800 Pa, head-on particle tracking confirms that the originally linear velocity profile takes a gooseneck shape, thus revealing shear banding. When the creep stress is stepped down to 100 Pa, this velocity profile evolves back to a linear one. The conclusion from this work is that even if nonlinear creep experiments are reproducible and a steady state is reached, this does not mean that the flow field is homogeneous.

Keywords Second normal stress difference · Instability · Necking · Polymer solution · Polystyrene · Particle tracking

This paper was presented at Annual European Rheology Conference (AERC) held in Hersonisos, Crete, Greece, April 27-29, 2006.

T. Schweizer (✉)
Department of Materials, ETH Zürich,
8093 Zürich, Switzerland
e-mail: thomas.schweizer@mat.ethz.ch

Introduction

Starting only recently to work with entangled polymeric solutions, we struggled over a series of papers (Tapadia and Wang (2004); Inn et al. (2005)) reporting on nonlinear shear creep experiments with highly entangled poly(butadiene) solutions (Z=33–50 entanglements per chain). Upon increasing the creep stress p_{21}, a transition at roughly $p_{21} \approx G_N^0/2$ is reported. When the creep stress is increased in this transition region by only 5%, the "steady-state" shear rate increases by two orders of magnitude. When the creep stress is decreased however, no such transition is observed. Tapadia and Wang (2004) explain their observation by an entanglement–disentanglement transition of the macromolecules, whereas Inn et al. (2005) argue for a runaway situation as a consequence of the loss of material by edge fracture, which, in a constant torque experiment, leads to a drastic increase of the shear rate due to the reduction of the effective cross-section.

Several departures from homogeneous viscometric flow have been experimentally confirmed and modeled. Among them, shear banding is the ability of a flowing fluid to form adjacent regions which have a shear-rate discontinuity at their interface. This can occur if the flow curve $p_{21}(\dot{\gamma})$ has a negative slope over some range of shear rates (Kumar and Larson (2000)). Shear banding is widely reported for solutions forming wormlike micelles (Britton and Callaghan (1997); Decruppe et al. (2001); Lerouge et al. (2006)). Techniques used to investigate shear banding are light scattering from the interface (Lerouge et al. (2006); Decruppe et al. (2001)), NMR microscopy (Britton and Callaghan (1997)), Laser Doppler velocimetry (Joo and Shaqfeh (1994)), small-angle neutron scattering (Terech and Coutin (2001)), and particle tracking velocimetry as employed in this study.

The aim of this paper is to show that the transitions found in poly(butadiene) systems are not observed in a particular polystyrene solution and that homogenous nonlinear creep experiments are only feasible in a very restricted shear stress range. A creep experiment is termed *nonlinear* if the resulting steady state shear rate $\dot{\gamma} > 1/\tau_d$, i.e., larger than the inverse reptation time. Polystyrene solutions cannot be prepared with the same number of entanglements per chain due to the much higher entanglement molecular weight of 18 vs 1.5 kDa for poly (butadiene). For a PS solution with Z=17.7, nonlinear creep experiments are reported. The homogeneity of the flow is checked by verifying the Cox–Merz relation and by means of particle tracking on the sample's surface. For comparison, experiments with the cone immersed in a sea of its own fluid will also be briefly discussed.

Experimental

The fluid used is prepared from PS powder (Polymer Laboratories) and diethyl phthalate (DEP). Its main features are summarized in Table 1, and the linear relaxation time spectrum is given in Table 2. The powder was stirred into the solvent and then left to equilibrate by diffusion at 60 °C in a tight glass jar during at least 2 months.

Rheological experiments in cone-plate geometry were performed on an ARES LR2 (TA Instruments, α=0.04 and 0.1 rad, tool diameter 25 mm) and an MCR 300 (Paar Physica, α=2, 4, and 6°, tool diameter 30 mm). The convection gas oven of the ARES was just able to maintain the measuring temperature of 25 °C. Upon prolonged illumination with a strong halogen lamp for video imaging, however, the temperature rose by several tenths of a degree. Nonlinear creep tests could only be performed up to a stress of about 600 Pa. Beyond this stress, the motor in the Inductosyn modus could not rotate fast enough for maintaining the set stress. The measuring temperature in the MCR 300 was controlled with a TEK 150P-C Peltier plate at 25±0.01 °C. The sample was loaded by means of two spatulas. The required mass of the sample was calculated from the known volume for complete gap filling for a density of the solution of 1.107 g/cm^3 at 25 °C. Thus, an overfilling of the gap and a consequent stripping of the edge could be avoided.

Optical observations were performed either tangentially (silhouette of edge) or head-on (particle tracking). A CCD camera connected to a tele-lens (FiberOptic, Model 30-450/C) was used for both. The ARES gas oven had two small windows. One of them was used to illuminate the background of the chamber for optimum contrast. For the MCR 300, a small hood with two windows to enclose the cone was built to reduce solvent evaporation during long-time experiments. Evaporation was monitored by performing frequency sweep tests before and after long-time runs. A Labview program allowed the determination of the radius of curvature of the edge as a function of time.

For particle tracking, bronze beads of diameter 50 μm were blown to the surface of the sample. Thus, only the motion of the outermost part of the sample was detected by directing the tele-lens perpendicular to the surface. Particle motion videos were analyzed by software written from Labview building blocks.

Table 1 Properties of the polystyrene solution PS2.6M16DEP

Property [unit]	Value
PS, M_w [kDa]	2,630
PS, M_w/M_n [–]	1.05
PS content [vol.%]	16
Z [entanglements/chain]	17.7
η_0 at 25 °C [Pa·s]	2,400
$J_{r,0}$ at 25 °C [Pa^{-1}]	$1.6 \cdot 10^{-3}$
τ_d [s]	3.8
G_N^0 [Pa]	2,700

Table 2 Relaxation time spectrum of the solution PS2.6M16DEP at 25 °C, calculated with the IRIS program, version 8.0

λ_i [s]	g_i [Pa]
0.000001001	228,500
0.0002314	1,628.33
0.001281	877.5
0.008216	684.75
0.04865	643.67
0.2512	639.67
1.206	515.17
5.404	268.33
22.01	5.7475

Results

Creep rheometry

For rheological systems not suffering from edge fracture, phase separation, slip, or deformation induced crystallization, a creep test is the most precise test at hand for stress-controlled rheometers. In the first phase of the test, a constant torque has to be maintained by the motor, the precision being limited by the thermal stability of the motor and the constancy of the current supply. In the second phase, no more energy is supplied to the sample and the recovery monitored. In this phase, the precision is given by the quality of the air bearing (residual torque) and the

resolution of the position measuring system. Inherent errors are that part of the elastically stored energy of the sample is used to move the tool and the rotor of the motor back and that the recovery is not free because the sample is hindered in its recovery in the axial direction.

In Fig. 1, the resulting shear rate is shown if the polystyrene solution PS2.6M16DEP is subjected to varying creep stresses between 100 and 2,500 Pa. For a stress of ≈100 Pa, normal stresses are first measurably beyond noise. The upper limit is close to the plateau modulus G_N^0 of the system of 2,700 Pa. Each data point in Fig. 1 is smoothed over its 51 neighbors. The maximum deformation is limited to 10 shear units for p_{21}<400 Pa and increases to 40 shear units for p_{21}=2,500 Pa. Larger deformations have been omitted to prevent the expulsion of fluid. After each creep experiment, the recovery was monitored during 20 min, which was enough to reach steady state. For p_{21}>800 Pa, the recovery was followed by an additional 30 min of rest for the edge of the sample to fully recover. Data for three different cone angles of 2, 4, and 6° are shown. By varying the cone angle, the gap at the edge changes between 0.52 and 1.57 mm. Figure 1 shows the following features: (a) The curves at a given stress are indistinguishable for the three angles within experimental error. (b) At stresses beyond 1,000 Pa, no steady shear rate is attained anymore. (c) There is no discontinuity in the steady-state shear rate while increasing the stress. Figure 2 shows the recoverable creep compliance J_r as a function of the stress applied during the first phase. The graph shows that within ±5%, J_r is constant and independent of α at $J_{r,0}=1.6\times10^{-3}$ Pa^{-1} up to 1,000 Pa. Then, after an upturn, J_r rapidly approaches zero. Figure 3 shows the verification of the Cox–Merz rule. The solid symbols are the steady shear rate from creep tests; the open ones are the steady shear stresses from step shear-rate experiments. Both kinds of tests have been performed on both rheometers and with different cone angles. This data is compared with $|G^*|(\omega)$ from frequency sweep experiments, performed at a strain amplitude of 3%.

The decrease of J_r in Fig. 2 is not a priori an indication for inhomogeneity. It could as well be due to disentanglement of the molecules. The discrepancy between the linear and nonlinear data in Fig. 3 however cannot be explained by entanglement effects. Because the effect is rather weak compared to the scattering of the data points, inhomogeneity has to be proven by yet another method.

Tangential view: shape of the sample's edge

All optical measurements shown in Figs. 4 and 5 have been performed on the MCR 300. The measuring geometry of the ARES LR2 with both tools being of the same diameter and with sharp edges would be more favorable for optical observations because the edge keeps much better its ideal shape. Unfortunately, experiments at constant stress are not possible beyond about 600 Pa. On the MCR 300 with only the cone being of a well-defined diameter and with a sharp edge, the solution tended to spread on the flat Peltier plate. This resulted in a slightly concave shape from the beginning, which was prone to start a crevice. Attempts to trim the edge with a plastic strip worsened the situation because it led to more wetting of the plate. First, in Fig. 4,

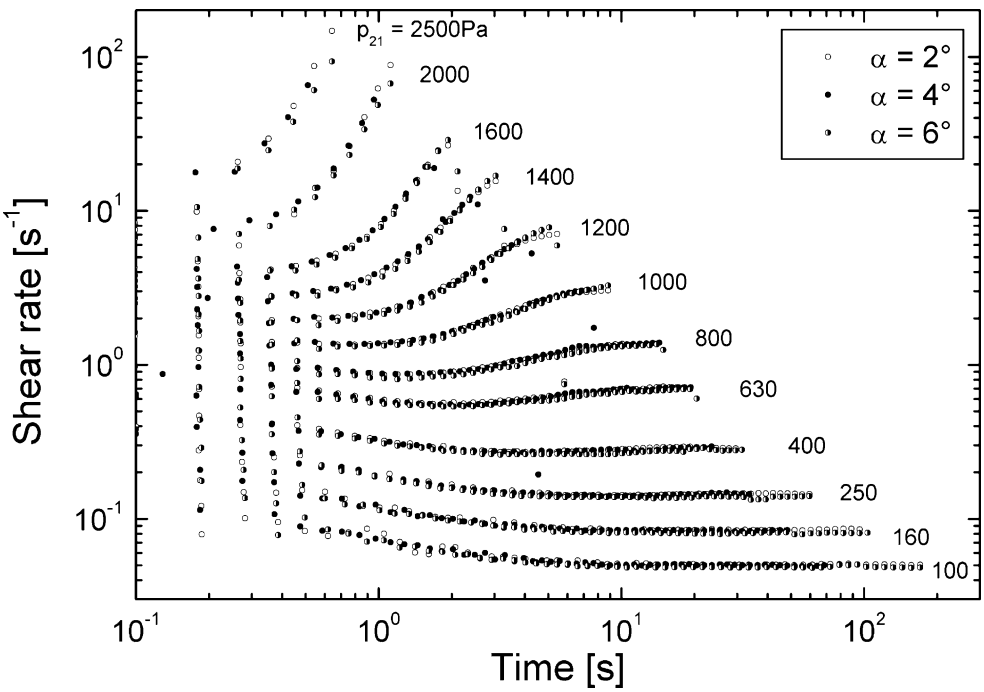

Fig. 1 Shear rate during creep test at stress given in the figure. Solution PS2.6M16DEP at 25 °C. MCR 300, cone-plate geometry with three different cone angles. The maximum strain is from 10 shear units at 100 Pa to 40 shear units at 2,500 Pa

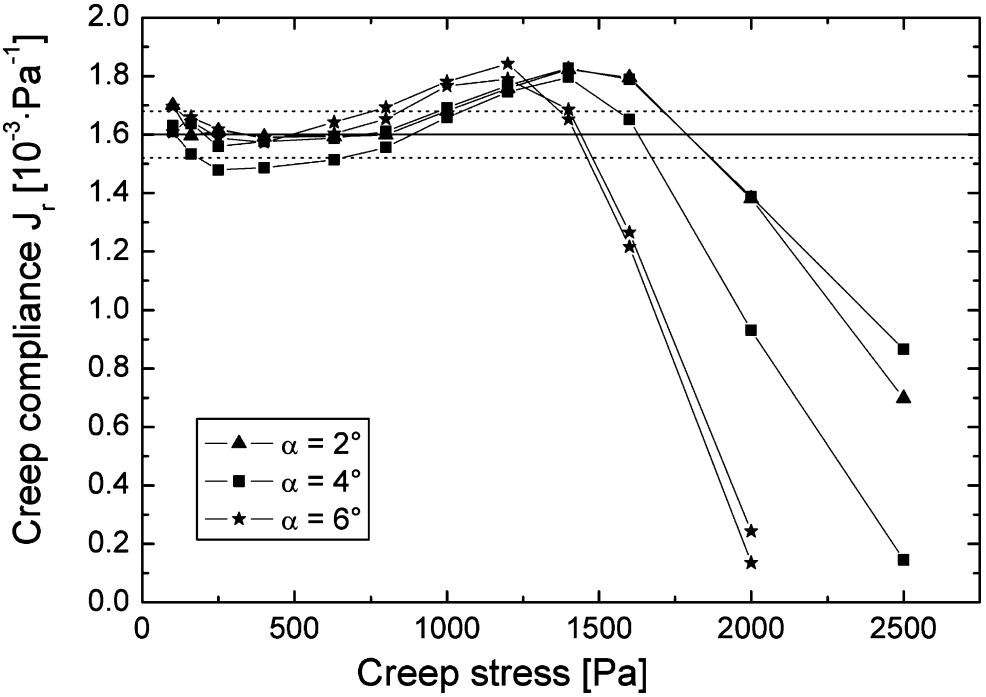

Fig. 2 Steady-state recoverable compliances of the creep tests shown in Fig. 1. The *lines* indicate the zero shear recoverable compliance $J_{r,0}=1.6\times10^{-3}$ $Pa^{-1}\pm5\%$. The steady-state values of J_r have been taken at $t'=200$ s

the evolution of the radius of curvature r_c was studied for three different creep stresses below and well above the threshold of $p_{21}\approx1{,}000$ Pa for steady-state flow. The radius of curvature at the tip of a sharp crevice is difficult to determine with the program at hand. It requires the definition of an observation sector. The radius of curvature is determined for the section of the edge lying within it. The edge is recognized from a preset black–white threshold. If the crevice becomes very deep and sharp, the section of the edge defined by the sector can no longer be fitted by a circle. In this case, a very small sector containing only the crevice has to be defined, with consequent difficulties in describing the early stage of the crevice formation. Figure 4 shows that even for the stress of 250 Pa for which a steady-state shear rate is smoothly approached, the initial radius of curvature r_c is only about 1.7 mm instead of the ideal 15 mm (radius of the tool). This is due to the spreading of the fluid as mentioned. Even at this low stress, the concave

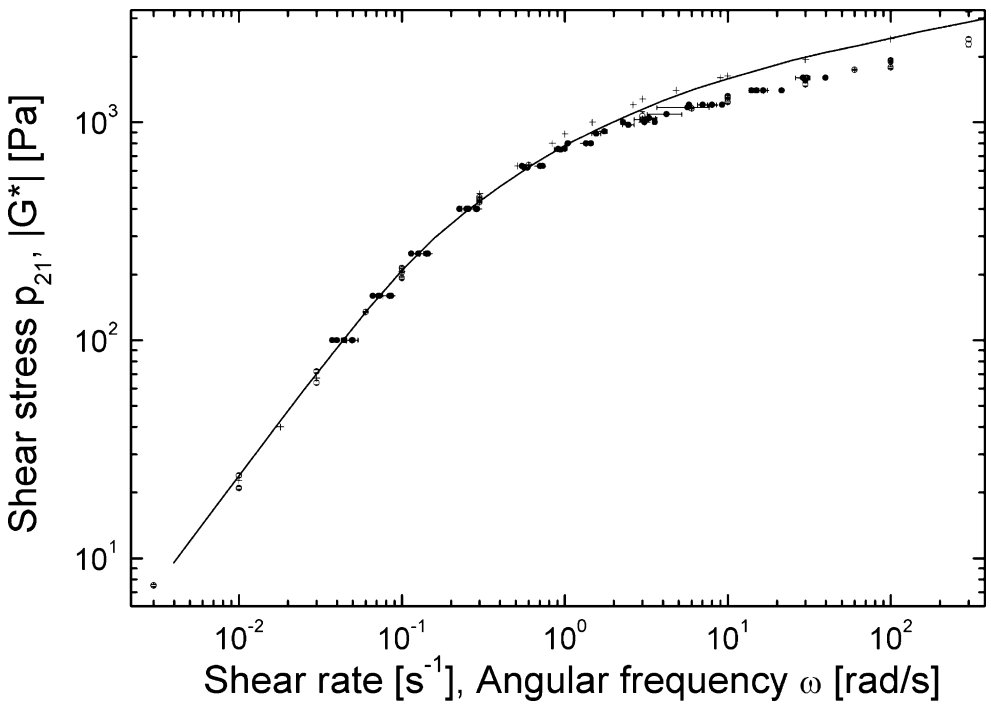

Fig. 3 Verification of the Cox–Merz rule. The *line* is $|G^*|$ from a frequency sweep test at 3% amplitude. *Solid symbols* are steady-state shear rates from creep experiments on the MCR 300 (cone angles 2, 4, and 6°) and the ARES LR2 (0.04 and 0.1 rad). On the ARES, the steady-state stress does not correspond to the set value beyond 600 Pa. The effective value is taken. The *open symbols* are steady-state stresses from step shear-rate experiments on the MCR 300 (cone angle 4°) and the ARES LR2 (0.1 rad). The *error bars* of the *open symbols* typically correspond to their size

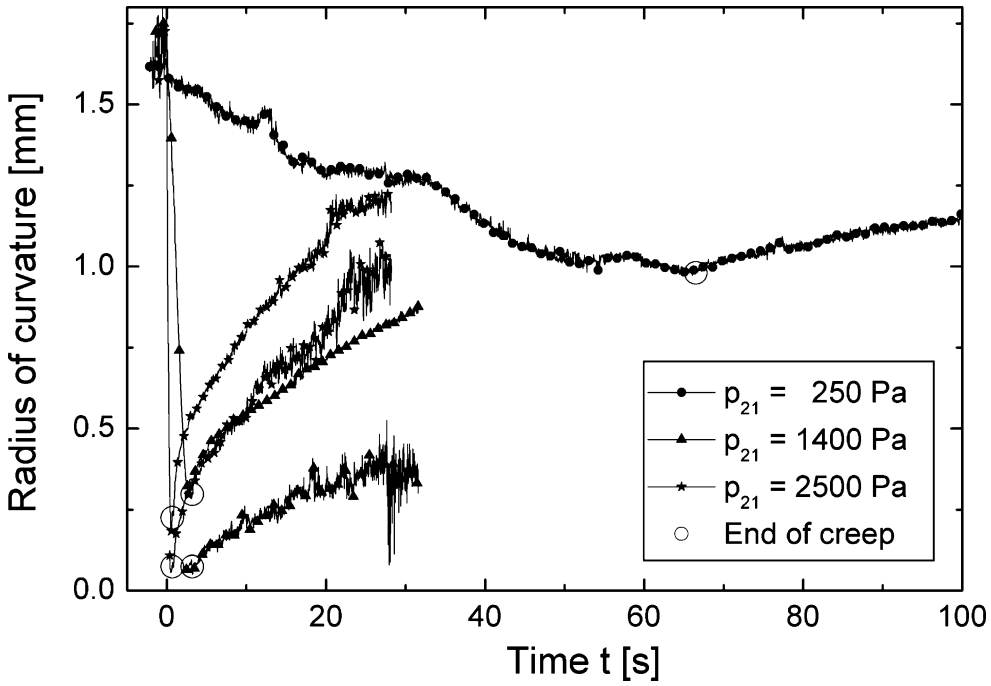

Fig. 4 Creep experiment with tangential observation of the edge. MCR 300 with a cone angle of 6°. The maximum strain is 10 shear units (p_{21}= 250 Pa) and 30 shear units (1,400 and 2,500 Pa). Shown is the radius of curvature at the most curved part of the edge. The edge shape is concave at the beginning and at all times during the experiment

shape of the edge sharpens to r_c=1 mm at 10 shear units. As soon as the flow is stopped, the surface tension starts to drive the surface contour back to its initial shape. For the two higher shear stresses of 1,400 and 2,500 Pa, the flow was stopped at 3.2 and 0.7 s, respectively, corresponding to 30 shear units. Within this short time, a very sharp crevice forms. The discrepancy between two repetitive tests is attributed to the problem of defining an appropriate sector to capture the section of the edge where the crevice is formed. After the flow is stopped, the crevice very quickly heals out—more quickly for the higher stress. The formation of this sharp crevice is a strong indication that the flow is inhomogeneous.

Head-on view: particle tracking

Because the radius of curvature at the tip and the depth of the crevice are difficult to quantify precisely, head-on views with analysis of the flow by particle tracking have been realized. The tele-lens was fully zoomed in so that the entire gap (1.05 mm for α=4°) filled the viewing area. Bronze particles of diameter 50 μm were blown to the surface of the sample with a plastic pipette as blowing tool. The particles were illuminated head-on in the plane of shear and from both sides of the tele-lens. With a Labview program, the particle motion was then analyzed. From the tracks of the particles obtained, the velocity of the surface of the sample as function of time and distance from the plate was calculated. Figure 5 shows the typical temporal evolution of the velocity profile during a creep test at 800 Pa. In Fig. 5a, at the beginning of the experiment, the velocity profile is linear. In Fig. 5b, when the flow is stopped at 40 shear units, the surface velocity shows a gooseneck-shaped distribution. This is a clear picture of shear banding. Two blocks are separated by a high shear plane. Now, the stress is stepped down to 100 Pa and the flow maintained for another 30 shear units. Figure 5c shows the velocity profile about 15 s after the step-down of the stress. Although the maximum speed is now an order of magnitude lower, the profile still shows the gooseneck shape. This means that the high shear layer from the larger stress still persists. Figure 5d shows the situation 12 min later at the end of this second stage. The velocity profile is almost back to linear. This means that the shear banding is not an irreversible process but that the molecules will start to reentangle in the high shear plane, provided that the flow is sufficiently slow and enough time is allowed. Plots of velocity vs distance from stationary plate require the knowledge of a scaling factor in pixels per millimeter and the exact location of the plate. Both of these quantities cannot be determined with the outmost precision. When looking at a grazing angle to the plate, there is low contrast to locate it. The edge of the cone is easier to locate. However, also, its position is blurred by some solutions covering the edge and reflecting light. The velocities in Fig. 5 have been calculated to the best of our possibilities. Another plot is provided in Fig. 6. Here, the shear rate at the inflection point of the velocity curve is plotted vs time. Calculating the shear rate does not require the knowledge of the scaling factors. The shear rate in the inflection point will coincide with the macroscopic averaged shear rate calculated from the rotation speed of the cone as long as the velocity profile is linear and there is no slip. Figure 6 shows that only up to about 10 s the flow can be considered

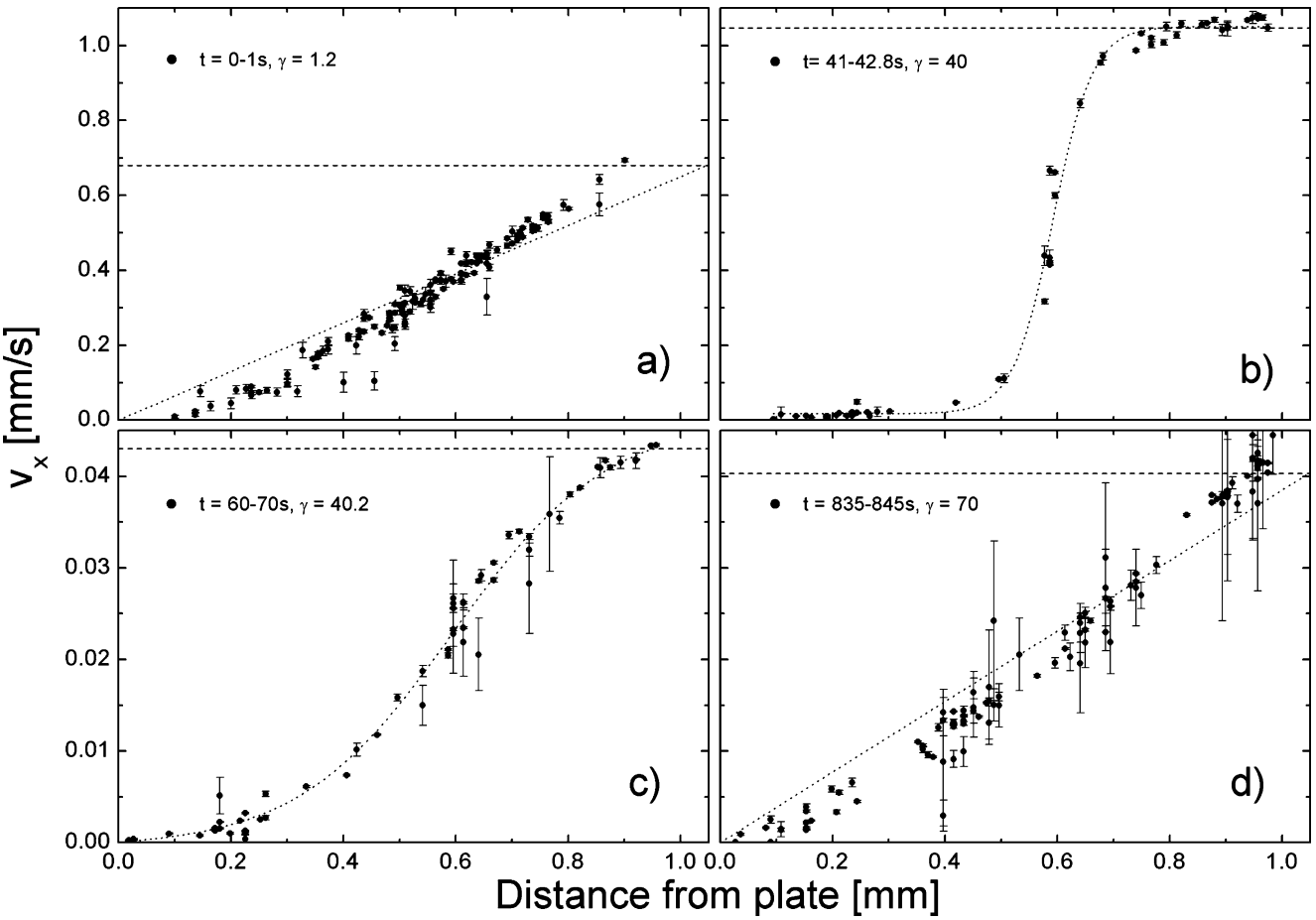

Fig. 5 Velocity profiles during creep at p_{21}=800 Pa followed by a step-down to 100 Pa. The step-down is at time 43.5 s (γ=40). **a** t=0–1 s, γ=1.2. **b** t=41–42 s, γ=38.5. **c** t=60–70 s, γ=40.2. **d** t=835–845 s, γ=70. Time spans indicate accumulated data for fitting. *Dotted lines* are: **a**, **d** linear fits, **b**, **c** Boltzmann fits. *Dashed lines* are: v_{Cone} (edge velocity) calculated from the rotational speed of the cone

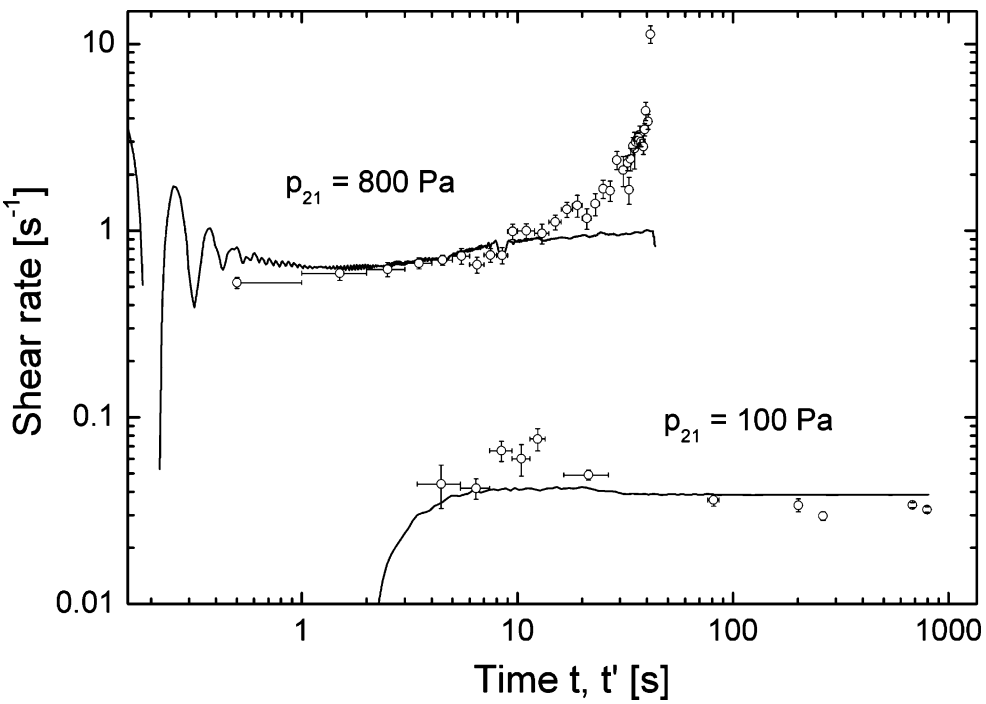

Fig. 6 Shear rate during creep test at p_{21}=800 Pa followed by a step-down to 100 Pa. Time t'=0 s at step-down for better readability. The *line* is the averaged shear rate from the rheometer; the *open circles* are the shear rates evaluated at the inflection points of v_x vs distance from plate as shown in Fig. 5

homogeneous. Then, the shear rate in the middle plane starts growing. Before the stress is decreased to 100 Pa at 43 s, the shear rate in the middle plane is an order of magnitude larger than the macroscopic one. There is no sign of $\dot{\gamma}$ (t) to level off, i.e., we already have a runaway situation at $\approx G_N^0/4$.

Discussion

The results show that the flow becomes clearly inhomogeneous beyond $p_{21} \approx 800$ Pa. This statement is based firstly on the nonobservance of the Cox–Merz rule and secondly on optical observation of the sample's surface.

How significant is the discrepancy found in Fig. 3? The few solid symbols with x-error bars from creep tests show that this data becomes quite unreliable in the regime where the discrepancy becomes most pronounced. The open symbols from step shear-rate experiments show their scatter in the stress-axis direction. In spite of that, both sets of data are within the same scatter band and clearly below $|G^*|(\omega)$. For a rheologically simple fluid of flexible molecules, the Cox–Merz rule is generally well obeyed. In a compilation of this rule, Dealy and Wissbrun (1990) found deviations only for some linear and branched polyethylenes and for rigid molecules. For other polymers, Booij and Palmen (1982) state that deviation from thermorheological simplicity can normally only be found if an extremely wide frequency range is covered. Therefore, the nonobservance of the Cox–Merz rule may be regarded as significant and indicative of an inhomogeneous flow situation. No conclusion can a priori be drawn whether this also involves edge fracture. Two attempts have been made to check this: immersion of the edge and optical observation.

The edge was immersed in its own fluid by a wall 2 mm away from the edge of the cone (compared to a gap opening in this case of 1.05 mm). A series of step shear-rate and creep experiments have been performed and the whole series shifted in the stress direction until correct values for the zero shear viscosity were obtained. This data is marked by the "+" symbol in Fig. 3. This data is much closer to $|G^*|(\omega)$, indicating a possible influence of the edge because any warping is suppressed by this method. Note, however, that nonlinear creep with an immersed cone is quite an undesirable experiment: The shear rate changes with time, and the shear stress is only known up to a factor. It is not even sure whether this factor is independent of shear rate.

The tangential observation of the edge leads to the conclusion that any kind of nonlinear shear experiment will lead to a change of the surface topology. Ideally, the surface should be part of a sphere centered on the rotation axis of the cone. Only for this boundary condition N_2 is equal at every point of the surface and N_1 is directly proportional to the normal force (Adams and Lodge (1964)). In practice, this condition is rarely met. For solutions, one usually starts with a concave surface, whereas for polymer melts, the edge is convex and $r_c \ll R$. Even by tempering and oversqueezing during loading, r_c cannot be increased substantially (Schweizer (2005)). As discussed above, the shape of the solution's edge in the MCR 300 gap is already slightly concave at the beginning. This is the reason why the velocity profile in Fig. 5a is not perfectly linear. During steady shear flow, there will be force equilibrium between the surface tension trying to drive the surface toward its equilibrium convex shape and the second normal stress difference trying to form a crevice because $|N_2|$ is maximal at the narrowest cross-section of the sample. At creep stresses below roughly 800 Pa, this equilibrium will be established and a stable surface with a concave shape results. As a consequence, the velocity distribution across the gap will no longer be linear as shown in Fig. 5b. At stresses >1,000 Pa, $|N_2|$ becomes too large—since concentrated at an increasingly sharp crevice—and cannot be compensated for by the surface tension. The minimum diameter of the sample will decrease, and the shear rate will grow rapidly. The crevice will become deeper and sharper. The shear is located in a thin layer at the narrowest cross-section, separating two blocks. Viscous heating will aggravate this.

The balance between the sample surface's tension and the second normal stress difference has been discussed in literature. Tanner (2002) came up with a condition for the crevice to propagate further:

$$|N_2| > \frac{2\sigma}{3r_c} \tag{1}$$

In steady state, $|N_2|$ is the pressure keeping the surface at a radius of curvature r_c. σ is the surface tension of the solution, assumed to be 40 mN/m. Because N_2 has not yet been measured for the fluid, two limiting curves are drawn in Fig. 7 for $|N_2|=0.1\cdot N_1$ and $|N_2|=0.2\cdot N_1$. $N_1(\dot{\gamma})$ are the steady-state first normal stress differences obtained from the creep tests in Fig. 1. Normal force measurements with small cone angles are critical. For the steady-state values of N_1, however, the compliance of the rheometers does not matter as discussed by Schweizer and Bardow (2005). The radius of curvature r_c in steady state is shown in Fig. 7. For the curve $p_{21}=250$ Pa in Fig. 4, the equilibrium radius is closely predicted. For the higher creep stresses, r_c fits as well, although an agreement cannot be expected: $|N_2|$ shows a sharp maximum at the tip of the crevice and Eq. 1 cannot be applied anymore.

Based on the results presented, the statement is made that there is no discontinuity in the curve $p_{21}(\dot{\gamma})$. Related to this, it has to be stressed that the maximum strain in Fig. 1 is between 10 and 40 shear units. The transitions discussed by

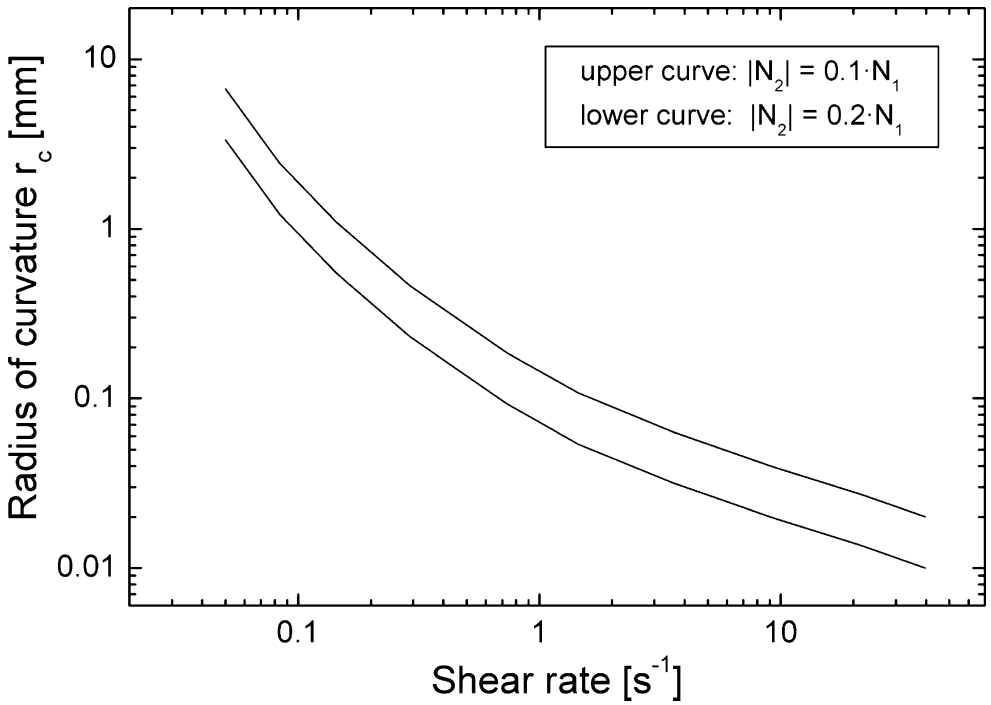

Fig. 7 Radius of curvature r_c of the concave edge of the sample. Calculated with Eq. 1, i.e., from the force balance between surface tension and $|N_2|$. The *two lines* represent Eq. 1 evaluated for $|N_2|=10$ and 20% of N_1, respectively. $N_1(\dot{\gamma})$ is obtained from the experiments shown in Fig. 1

Tapadia and Wang (2004) and Inn et al. (2005) occurred at strains of several 100 to 1,000 shear units. It has been reported that transitions can occur after longer periods of steady shear in poly(isobutylene) Boger fluids (Magda and Larson (1988); McKinley et al. (1991)). However, if a fluid is sheared for several 1,000 shear units, some departures from the original type of flow will certainly occur by viscous heating (Bird and Turian (1962)), chain degradation (Laun and Hingmann (1990)), or pressure fluctuations (Lodge (1961)).

Figure 1 shows that as long as $p_{21}<800$ Pa, 10 shear units is enough to reach steady state. It was found little plausible that the strain to reach steady state should increase by orders of magnitude for the higher stresses. Because of this, to prevent the expulsion of fluid, and to control a runaway situation, the flow was always stopped at strains < 40 shear units.

Conclusions

(a) Nonlinear creep experiments with entangled polystyrene solutions can be performed but not on all rheometers. Up to $p_{21}\approx G_N^0$ that there is no discontinuity if the steady-state shear rate or the rate at the final strain of 40 shear units is plotted vs the creep stress. Within experimental resolution, the gap ($=\alpha\cdot R$) does not have an influence on the steady-state shear rate. Beyond about $G_N^0/4$, there is no steady shear rate anymore.

(b) The flow becomes inhomogeneous for $p_{21}>G_N^0/4$. This is quantitatively seen by the nonobservance of the Cox–Merz rule. More clearly, surface particle tracking reveals a departure from the linear velocity profile. This is accompanied by the growth of a crevice, narrowing the cross-section, as seen by observing the silhouette of the edge. At $p_{21}>G_N^0/4$, a high shear plane separates two blocks of material being stationary or moving with the speed of the cone. The geometry of the rheometer used (cone with $R=15$ mm and flat plate) proved to be unfortunate for this kind of experiments because it presets a concave shape of the sample's edge. During creep in the range $G_N^0/4<p_{21}<G_N^0/3$, although the flow is inhomogeneous, a steady state is observed. There is equilibrium between the second normal stress trying to deepen the crevice and the surface tension of the solution opposing it.

(c) Upon cessation of flow, the surface tension quickly restores the original shape of the edge. The fluid can thus be used for several consecutive experiments.

(d) No loss of fluid was observed from the gap. It is assumed, however, that during the formation of the crevice, the excess fluid is used to increase the wetting radius on the plate.

(e) Nonlinear creep flow with polymer fluids at $p_{21}>G_N^0/3$ is an unstable experiment. Because narrowing of the sample's cross-section is inevitable, the constant torque will lead to runaway.

(f) Immersing the cone in a sea of its own fluid will prevent the narrowing of the cross-section, but it

cannot avoid inhomogeneous flow. The high shear plane will propagate from the surface of the sea.

Acknowledgment The author wishes to thank Fredy Mettler for his support with the adaptation and optimization of the Labview programs and Marina Karlina for her help with the experiments. The financial support of ETH Zurich for this project is gratefully acknowledged.

References

Adams N, Lodge A (1964) Rheological properties of concentrated polymer solutions II. A cone-and-plate and parallel plate pressure distribution apparatus for determining normal stress differences in steady shear flow. Phil Trans R Soc Lond Ser A 256 (1068):149–184

Bird RB, Turian RM (1962) Viscous heating effects in a cone and plate viscometer. Chem Eng Sci 17:331–334

Booij HC, Palmen JHM (1982) Some aspects of linear and nonlinear viscoelastic behaviour of polymer melts in shear. Rheol Acta 21:376–387

Britton MM, Callaghan PT (1997) Two phase shear band structures at uniform stress. Phys Rev Lett 78:4930–4933

Dealy JM, Wissbrun KF (1990) Melt rheology and its role in plastic processing. Reinhold, New York

Decruppe JP, Lerouge S, Berret JF (2001) Insight in shear banding under transient flow. Phys Rev E Stat Nonlin Soft Matter Phys 63 (2 Pt 1):022501

Inn YW, Wissbrun KF, Denn MM (2005) Effect of edge fracture on constant torque rheometry of entangled polymer solutions. Macromolecules 38:9385–9388

Joo JL, Shaqfeh ESG (1994) Observations of purely elastic instabilities in the Taylor–Dean flow of a Boger fluid. J Fluid Mech 262:27–73

Kumar S, Larson RG (2000) Shear banding and secondary flow in viscoelastic fluids between a cone and plate. J Non-Newton Fluid Mech 95:295–314

Laun HM, Hingmann R (1990) Rheological characterization of the fluid M1 and of its components. J Non-Newton Fluid Mech 35:137–157

Lerouge S, Argentina M, Decruppe JP (2006) Interface instability in shear-banding flow. Phys Rev Lett 96:0883001-1-4

Lodge AS (1961) Rheological properties of concentrated polymer solutions I. Growth of pressure fluctuations during prolonged shear flow. Polymer 2:195–201

Magda JJ, Larson R (1988) A transition occurring in ideal elastic liquids during shear flow. J Non-Newton Fluid Mech 30:1–19

McKinley G, Byars JA, Brown RA, Armstrong RC (1991) Observations on the elastic instability in cone-and-plate and parallel-plate flows of a polyisobutylene Boger fluid. J Non-Newton Fluid Mech 40:201–229

Schweizer T (2005) Rupture de polymères fondus lors d'un écoulement de cisaillement. Actes 40ème Coll. Annuel Groupe Français de Rhéologie, Nice

Schweizer T, Bardow A (2005) The role of instrument compliance in normal force measurements of polymer melts. Rheol Acta 45 (4):393–402

Tanner RI (2002) Engineering rheology, 2nd edn. Oxford University Press, Oxford, UK

Tapadia P, Wang SQ (2004) Nonlinear flow behaviour of entangled polymer solutions: yieldlike entanglement–disentanglement transition. Macromolecules 37:9083–9095

Terech P, Coutin A (2001) Organic solutions of monomolecular organometallic threads. Nonlinear rheology and effects of end-capping species. J Phys Chem B 105(24):5670–5676